

Inertia-Gravity Waves in the Stratosphere

TIMOTHY J. DUNKERTON

Physical Dynamics, Inc., Bellevue, WA 98009

(Manuscript received 16 January 1984, in final form 20 September 1984)

ABSTRACT

The propagation and refraction of stationary inertia-gravity waves in the winter stratosphere is examined with ray tracing. Due to their smaller vertical group velocity these waves experience more lateral ray movement and horizontal refraction than the simple gravity waves recently discussed by Dunkerton and Butchart. Stationary waves are rotated by the transverse horizontal shear and propagate into the polar night jet. Circumstances are found in which the mean flow shear has enhanced unstable wavebreaking by compressing the wave packet and decreasing the absolute value of wave action density required for breaking. In some other places, reflection from the caustic is more likely.

1. Introduction

Recently the author performed three-dimensional ray tracing calculations to determine the effect of sudden warmings on gravity wave propagation through the winter stratosphere (Dunkerton and Butchart, 1984). We confined attention to the simple non-inertial and hydrostatic waves of horizontal scale 50–200 km which appear to be dominant in mesospheric radar data (e.g., Vincent and Reid, 1983; Fritts, 1984). It was recognized in our paper that although lateral ray movement and horizontal refraction are often secondary effects for simple gravity waves propagating vertically in the stratosphere, such would not be the case for inertia-gravity waves with smaller vertical group velocity. These waves are observed in the mesosphere, less frequently, perhaps, than simple gravity waves (Smith and Fritts, 1983). On the other hand there is growing evidence of a stratospheric fine structure due to inertia-gravity waves (Sawyer, 1960; Thompson, 1978; Cadet and Teitelbaum, 1979; Sato and Woodman, 1982; Barat, 1983; Yamanaka and Tanaka, 1984a).

As a sequel to Dunkerton and Butchart (1984) this paper briefly examines the propagation and refraction of stationary inertia-gravity waves in the winter stratosphere for waves of initial scale up to 800 km. Linear theory allows vertical propagation when

$$f^2 < \hat{\omega}^2 < N^2, \quad (1.1)$$

where f is the Coriolis parameter, $\hat{\omega} = \omega - \mathbf{k} \cdot \bar{\mathbf{u}}$ is intrinsic frequency, and N is Brunt-Vasala frequency. In winter the mean wind in extratropical latitudes is normally westerly, favoring the vertical propagation of stationary hydrostatic waves for which $|\mathbf{k} \cdot \bar{\mathbf{u}}| > |f|$ (Lindzen, 1981).

Of particular interest in this problem is the effect of transverse horizontal shear. Understandably the *vertical shear problem* has received much attention (Jones, 1967; Grimshaw, 1975, 1980; Yamanaka and Tanaka, 1984a,b). Generalizations including horizontal shear have appeared elsewhere (Jones, 1969; Acheson, 1973; Ivanov and Morozov, 1974; Mooers, 1975a,b; Olbers, 1981). But as Olbers notes, these models make simplifying assumptions, e.g., constant shear, which can be of only qualitative use in geophysical flows, if at all.

For this reason it is preferable to solve the ray tracing equations numerically. These equations, derived in Section 2 for hydrostatic inertia-gravity waves, are solved in Section 3 using the Dunkerton and Butchart (1984) code and an analytical model of unidirectional mean winds. A few illustrative examples are considered. A notable feature of these ray tracing results is the refraction of stationary waves into the polar night jet.

Section 4 examines the unstable breakdown of inertia-gravity waves using a simple model of wave action conservation. As long as the ray tracing approximation remains valid, wavebreaking is enhanced in those regions where wave packet compression occurs and the absolute value of wave action density required for wavebreaking decreases. A favored location for breaking would seem to occur above the tropospheric jet stream as stationary waves are refracted into the polar night jet. Wavebreaking in or below the polar night jet may be contrasted to the situation for simple gravity waves, which for the most part are expected to break above the jet on normal undisturbed winter days (Lindzen, 1981; Holton, 1982; Dunkerton, 1982a,b), and for planetary Rossby waves, which in the stratosphere tend to break equa-

toward of the jet (McIntyre, 1981; McIntyre and Palmer, 1983).

2. Ray tracing for hydrostatic inertia-gravity waves

The reader is referred to Lighthill (1978) for a general introduction to ray tracing in a wind. Let d/dt denote the time rate of change following a ray, and assume a dispersion relation of the form

$$\omega = \omega(k_i, x_i), \quad (2.1)$$

where ω is wave frequency, k_i is total wavenumber, and x_i is the three-dimensional space coordinate. The ray tracing equations then assume the general form

$$dx_i/dt = (\partial\omega/\partial k_i)_{x_i}, \quad (2.2a)$$

$$dk_i/dt = -(\partial\omega/\partial x_i)_{k_i}. \quad (2.2b)$$

For hydrostatic inertia-gravity waves the dispersion relation is

$$\hat{\omega}^2 = \frac{N^2 K^2}{m^2} + f^2, \quad (2.3)$$

where K is total horizontal wavenumber and m denotes vertical wavenumber. Ray tracing for hydrostatic inertia-gravity waves on a zonal mean zonal flow was discussed by Kitchen and McIntyre (1980). A slight generalization of their results to include a mean meridional flow \bar{v} and zonal variation of the mean flow yields

$$u_g = \bar{u} + \frac{kN^2}{\hat{\omega}m^2} \quad (2.4a)$$

$$v_g = \bar{v} + \frac{lN^2}{\hat{\omega}m^2} \quad (2.4b)$$

$$w_g = -\frac{N^2 K^2}{\hat{\omega}m^3}, \quad (2.4c)$$

where u_g , v_g , and w_g denote zonal, meridional, and vertical components of \mathbf{c}_g , the three-dimensional vector group velocity. The horizontal refraction for horizontally constant $N(z)$ is given by

$$dk/dt = -(k\bar{u}_x + l\bar{v}_x), \quad (2.5a)$$

$$dl/dt = -\left(k\bar{u}_y + l\bar{v}_y + \frac{\beta f}{\hat{\omega}}\right), \quad (2.5b)$$

where k and l are the zonal and meridional components of the wavevector k_i , orthogonal to wave crests, and $\beta = df/dy$. Effects of the spherical coordinate system (Dunkerton and Butchart, 1984) are added to (2.5) but are generally small in the examples considered here.

The refraction equation for m is redundant with the dispersion relation (2.3). In this paper we assume moreover that $N = 0.02 \text{ s}^{-1}$, constant in height, and that the mean flow is temporally constant. Time-

dependence may be important in the middle atmosphere, particularly for very long inertia-gravity waves prior to a sudden warming, and contributes to changes in absolute frequency along the lines discussed by Jones (1969). This effect is neglected here.

3. Inertia-gravity waves in realistic winds

a. In three dimensions

The ray tracing algorithm (Dunkerton and Butchart, 1984) may be initialized with stationary waves of long horizontal wavelength, including modifications for rotation. Due to the greater amount of lateral ray movement and horizontal refraction the results are generally more difficult to interpret, however. Here we present the results of one such simulation using stationary waves of 800 km initial zonal wavelength. Three-dimensional geostrophic winds for 17 January 1979 were borrowed from Dunkerton and Butchart (1984), shown in Fig. 1. The reader may refer to that paper for other details.

In Fig. 2 it is apparent that most of the surviving rays reaching the stratopause on this day arrive there in the vicinity of the polar night jet. Their vertical propagation is favored in regions of strong mean winds. The climatological pattern, evident over the North Pacific on this day, involves a tropospheric jet stream equatorward of the overlying polar night jet. In this configuration the rays are bent to the north, into the jet, while being advected to the east with the mean flow. Obviously the waves can travel several thousand kilometers horizontally through the stratosphere, even though their phase propagation is identically zero. Moreover these surviving rays are not victims of radiative dissipation since our model includes a short-wave cutoff using Fels' (1982) scale-dependent radiative damping.

Closer inspection of these results, and those for waves of initially longer horizontal scale, revealed that rays initially lying on different latitude circles would often cross paths on their way to the stratopause. Ray overlapping was a minor feature in Dunkerton and Butchart (1984). Its prevalence in these cases suggests that the ray tracing formalism should be used with extreme caution for inertia-gravity waves.

b. Two-dimensional analytic wind profile

To better understand ray racing of inertia-gravity waves, some simplification was desirable. Recognizing that the mean flow is rotational rather than deformational in character, mainly due to \bar{u}_y , the author subsequently adopted an analytic profile of stratospheric winds, assumed unidirectional. From Jones (1969) and others we infer that the wavevector component parallel to a unidirectional flow remains constant. The simulation of Fig. 2, also confirms that k is fairly constant, apart from small effects due to

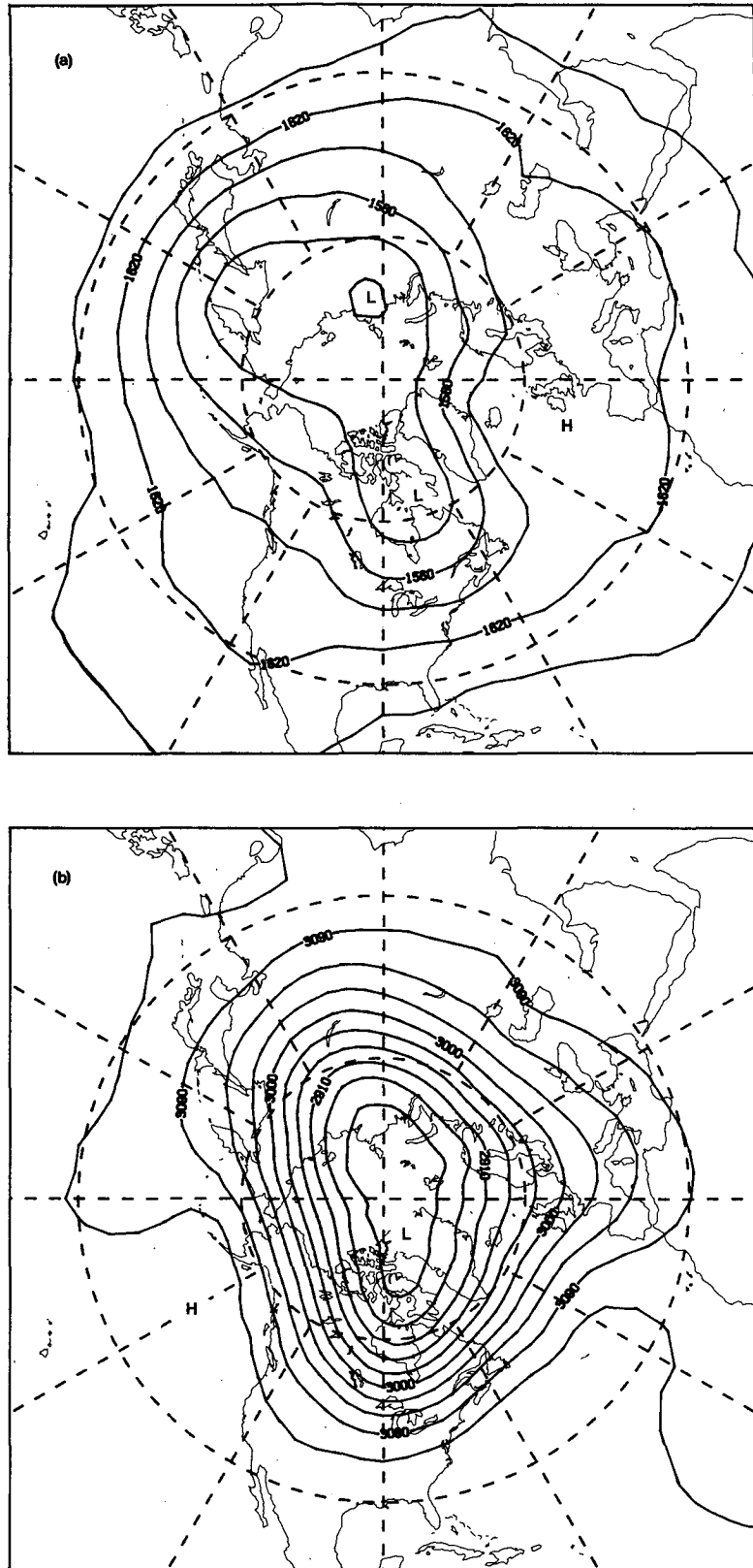


FIG. 1. Geopotential height fields (dm) derived by inversion of satellite radiance data for 17 January 1979 at 100, 10, and 1 mb.

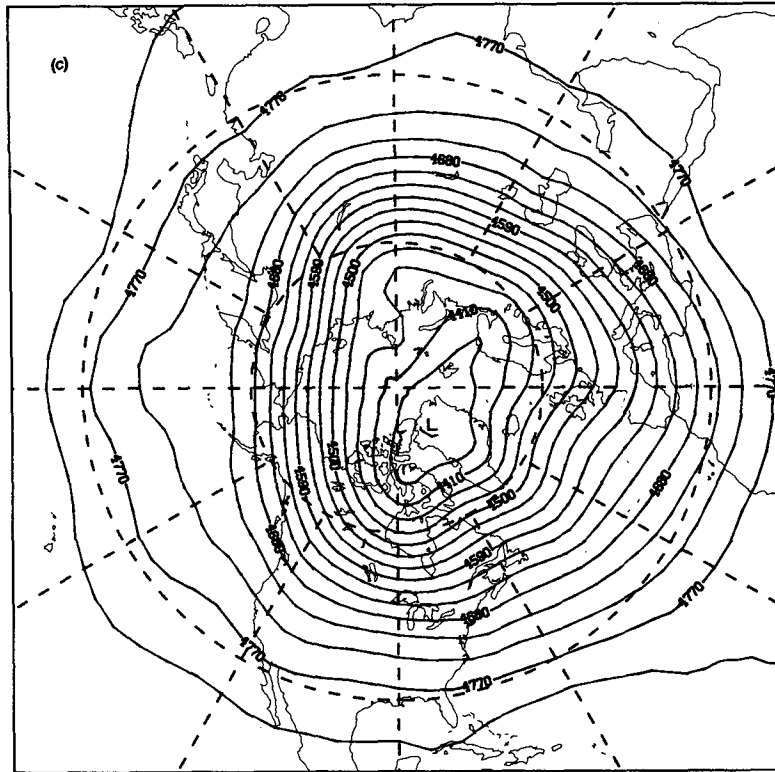


FIG. 1. (Continued)

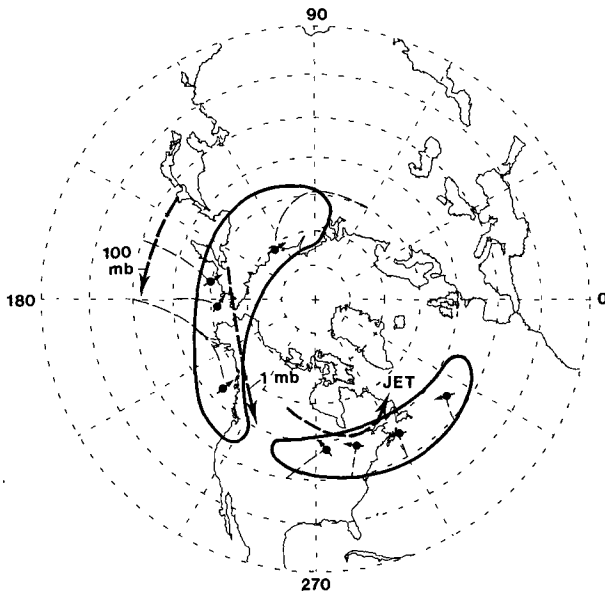


FIG. 2. Final positions and orientations for selected inertia-gravity wave rays propagating in the three-dimensional winds of Fig. 1. Heavy contour outlines the region on the 1 mb surface containing over 95% of the surviving rays in this simulation. Thin dashed lines connect initial and final positions for selected rays. Initial wave parameters are 800 km zonal wavelength ($l = 0$) and stationary waves.

zonal variations. The transverse components, on the other hand, would undergo something like linear variation in time. In this case Jones' "taffy-pull" illustration, appropriate for waves in a deformational flow, may be replaced with a "Venetian blind" analogy. The differential advection of wave phase in a rotational flow can be visualized by opening and closing such a device, seen edge-on.

Using an analytic profile circumvents the need for interpolation between data grid points. The main problem, as always, is to find a representative \bar{u} . In the following discussion we assume a unidirectional mean wind in the x -direction of the form

$$\bar{u}(\theta, z) = \bar{u}_m(z) \exp - \left(\frac{\theta - \theta_m(z)}{\theta_0(z)} \right)^2 + \bar{u}_0 \quad (3.1)$$

where θ is latitude and

$$\bar{u}_m(z) = 20 \text{ m s}^{-1} \left\{ 2 + \tanh \frac{z - 28 \text{ km}}{7 \text{ km}} \right\} \quad (3.2a)$$

$$\bar{u}_0 = 5 \text{ m s}^{-1} \quad (3.2b)$$

$$\theta_m(z) = 58^\circ - 18^\circ \left\{ \frac{z - 34 \text{ km}}{24 \text{ km}} \right\}^2 \quad (3.2c)$$

$$\theta_0(z) = 20^\circ + 5^\circ \times \left\{ \tanh \frac{z - 10 \text{ km}}{7 \text{ km}} + \tanh \frac{z - 50 \text{ km}}{7 \text{ km}} \right\} \quad (3.2d)$$

in the range $20^\circ \leq \theta \leq 80^\circ$, $10 \text{ km} \leq z \leq 50 \text{ km}$. This profile resembles the zonally-averaged zonal wind above 100 mb on 17 January 1979. Of course we do not regard the zonal mean flow as having any value for ray tracing when planetary waves are present, but rather adopt this profile as a typical *local* polar night jet. Strictly speaking the x -direction is now taken parallel to the jet, and so on. Other profiles found in Fig. 1 would give different results. For example, stronger mean winds would allow vertical propagation for stationary waves of longer horizontal scale. Another scenario of some practical interest involves propagation into negative shear above the tropopause (e.g. Yamanaka and Tanaka, 1984a). Negative \bar{u}_z is found in (3.1) in a small region south of 40°N . and below 25 km.

c. Some results

The discussion now ignores dissipative effects, in the spirit of a more usual ray tracing calculation. Ray positions are initialized at 10 km elevation in 1° latitude intervals from 20 to 80°N . Figure 3 displays ray trajectories for the first case:

$$\omega = 0, \quad (3.3a)$$

$$k = 2\pi (400 \text{ km})^{-1}, \quad (3.3b)$$

$$l_0 = 0, \quad (3.3c)$$

where the zero subscript denotes the initial value. Refraction into the polar night jet is the obvious feature in Fig. 3. Quite by accident, this first simulation provided a spectacular example of two entirely different kinds of ray behavior. To the left of the "ray cone" the rays are confluent and seem to be overlapping onto the same characteristic. Rays furthest to the left have the slowest vertical group velocity, being in the weakest winds, and acquire the largest meridional wavenumber. Closer inspection of these results indicated that *in this particular case* the latitudinal separation between adjacent rays remained finite all the way to the stratopause. Moreover the rate of change of meridional (vertical) wavenumber over a meridional (vertical) wavelength also remained small; the ray tracing approximation seems uniformly valid on this side of the cone. The resulting behavior may be likened to that of generalized critical layer (see below). The minimum refraction-induced meridional wavelength is about 90 km at the stratopause for the southernmost ray shown.

Things are very different on the right side of the cone. There are about five instances of ray overlapping shown here, forming the well-known "caustic" (e.g., Lighthill, 1978, Fig. 98). Ray tracing predicts infinite

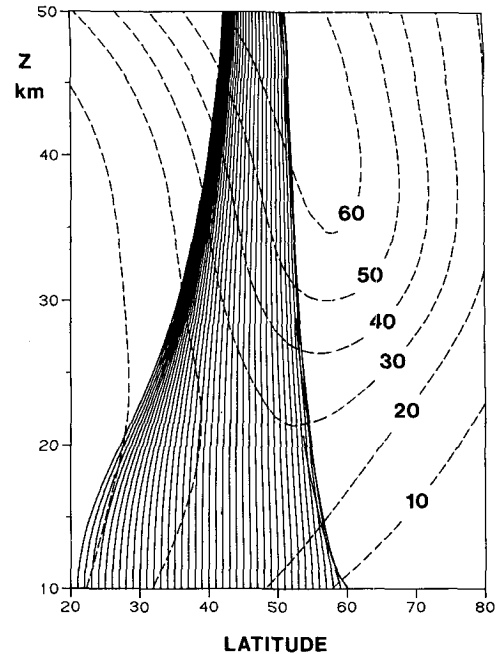


FIG. 3. Ray propagation in the analytic unidirectional mean wind profile for the case $\omega = 0$, $k = 2\pi (400 \text{ km})^{-1}$, and $l_0 = 0$.

wave amplitude in a finite time and violates its own assumptions of slowly-varyingness at the caustic. In practice, we would not expect ray tracing to very accurate at the extreme right of the cone.

As a slight variation of this experiment Fig. 4 traces rays for waves of initial NW-SE wavevector orientation:

$$\omega = 0, \quad (3.4a)$$

$$k = 2\pi (400 \text{ km})^{-1}, \quad (3.4b)$$

$$l_0 = -k. \quad (3.4c)$$

Rays slant further to the north, as does the left side of the cone as a whole. Also the vertical group velocity is initially $\sqrt{2}$ smaller. Otherwise the behavior is similar.

In both Figs. 3 and 4 the inertial frequency cutoff inhibits vertical propagation north of 60°N . Aside from this, however, rotation is usually a small effect in these examples. When the experiment of Fig. 3 was repeated with $f \equiv 0$, the left side of the cone moved about 2° to the south (i.e., slightly less horizontal refraction).

Figure 5 shows an example of more distinctly *inertia-gravity* waves:

$$\omega = 0, \quad (3.5a)$$

$$k = 2\pi (800 \text{ km})^{-1}, \quad (3.5b)$$

$$l_0 = 0. \quad (3.5c)$$

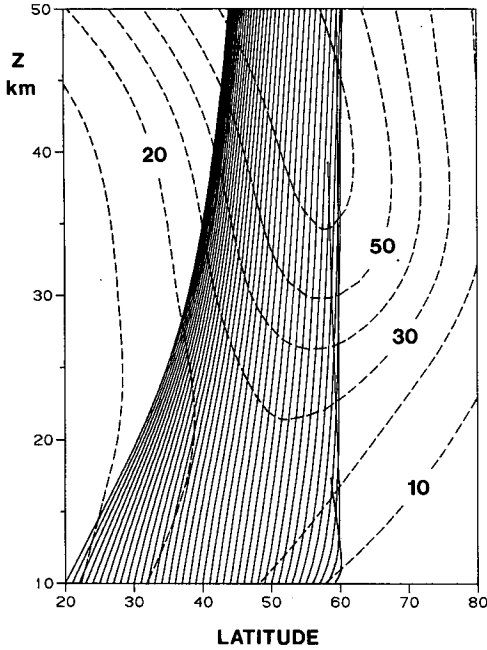


FIG. 4. As in Fig. 3 but for $l_0 = -k$.

The ray cone resembles a twisted piece of ribbon. The caustic is now traced out by the majority of rays, and is present also at the left side of the cone between 20 and 25 km. At the stratopause the order of rays is reversed, a two dimensional example of the crossing of ray paths mentioned in Section 3a above. Over most of Fig. 5 the ray tracing approximation is inadequate unless reflection is taken into account.

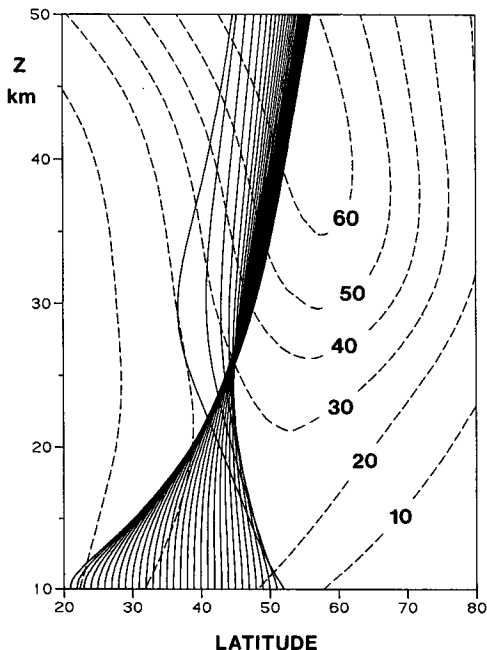


FIG. 5. As in Fig. 3 but for $k = 2\pi (800 \text{ km})^{-1}$.

4. Wave action conservation

a. Ray time and its implications

Up to this point nothing explicit has been said about the *ray time*, the amount of time required for a ray to propagate to a given point in Figs. 3–5. It is appropriate to begin our discussion of wave action conservation by first looking at this quantity in one particular case.

Figure 6 reproduces the experiment of Fig. 3, showing the same rays together with contours of ray time up to 12 h. An additional contour at $t = 24$ h is also shown. At once it is apparent that radiative damping is irrelevant for the majority of rays originating in the band $25^\circ \leq \theta \leq 55^\circ$. Ray times are well below the radiative damping time scale in this region, even when the weakly scale-dependent rates of Fels (1982) are taken into account.

The contours of ray time have a more important function, allowing the viewer to deduce something about wave action behavior. For conservative waves,

$$\frac{\partial A}{\partial t} + \frac{1}{\rho_0} \nabla \cdot \rho_0 \mathbf{c}_g A = 0, \quad (4.1)$$

where $A = E/\hat{\omega}$, E is wave energy density, $\rho = \rho_0 \times \exp -z/H$ is basic state density, and \mathbf{c}_g is the three-dimensional vector group velocity (Andrews and McIntyre, 1978). Solution of (4.1) requires an

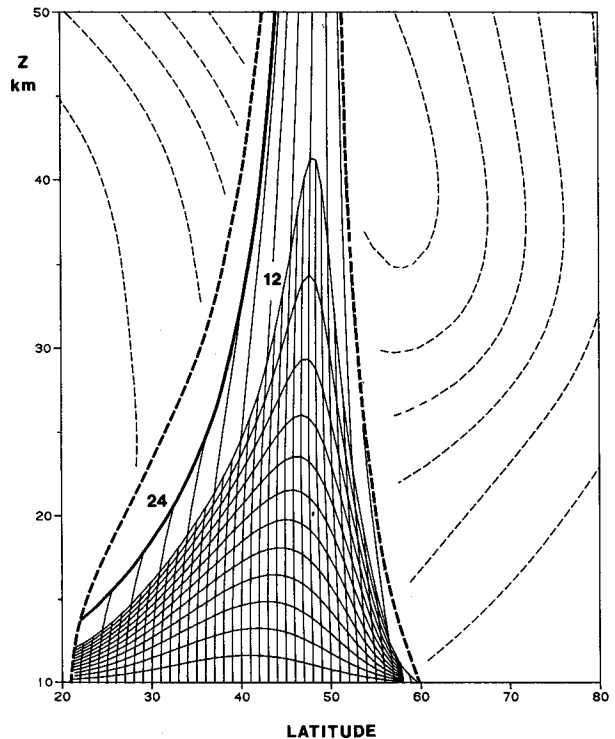


FIG. 6. Contours of ray time in 1 h intervals superimposed on the ray trajectories of Fig. 3.

initial and boundary condition. However, imagine a simple case (not very realistic by WKB standards) in which a rectangular wave packet of 1 hour duration and 1° latitude width is forced at the lower boundary. Each rectangle in the overlying column, or ray tube, then represents the packet at one hour intervals. Note that rectangles north of about 42°N . grow with height while those to the south are compressed. Accordingly the packet-integrated, density-weighted wave action $\langle \rho_0 A \rangle$ will grow (decay) with time as the packet undergoes compression (expansion). At the left of the cone we then have another motive for likening the behavior to that of a generalized critical layer. On the other hand, the divergent behavior at the center of the cone resembles that found in positive vertical shear studied by Lindzen (1981), Dunkerton (1982a) and others.

b. Convective wavebreaking

Given enough information it would be straightforward to determine if the mean flow shear has helped the wave action density satisfy the marginal criterion for instability to local convection. Unfortunately the calculation is amplitude-dependent; lacking better observational guidance, only qualitative remarks can be made. For the most part the waves in Fig. 6 are adequately far removed from the inertial frequency so that the waves in question are basically simple gravity waves. Following the various derivations of Lindzen (1981), Holton (1982), and Dunkerton (1982a) the simple gravity wave is marginally stable to local convection when

$$A = A_s \equiv \frac{1}{2} \frac{N^2}{\hat{\omega} m^2} = \frac{1}{2} \frac{\hat{\omega}}{K^2}. \quad (4.2)$$

Below 30 km and south of 40°N ., $|A_s|$ decreases along a ray, due mainly to the lateral shear which has increased K , and also to the negative vertical shear which has decreased \bar{u} . Towards the center of the cone $|A_s|$ evolves in the opposite and more familiar sense in the stratosphere: K is reasonably constant and \bar{u} is increasing with height along a ray. Wavebreaking is not, therefore, expected at the center of the cone (Dunkerton, 1982a), nor for that matter in the vicinity of the caustic. The situation at the left of the cone above 40 km is more ambiguous as the effects of vertical and horizontal shear conflict.

c. Dynamical wavebreaking

Similar remarks apply to the example of 800 km waves shown in Fig. 5, although the region of enhanced wavebreaking based on ray tracing is restricted to below 20 km. Irrespective of the validity of ray tracing there are a few additional comments to be made.

First, when rotation is important there is a distinct possibility of Kelvin-Helmholtz instability in the local wave + mean field. Derivation of a "dynamically saturated" wave action density \tilde{A}_s is given in the Appendix. This situation may be contrasted to that of simple gravity waves: any convectively stable simple gravity wave satisfies $\text{Ri} \geq \frac{1}{2}$ (where Ri is the local Richardson number) when \bar{u}_z is small, as in the WKB approximation.

We note in passing that KH instability is a special kind of nonlinear interaction whereby a large-amplitude inertia-gravity wave may undergo "breaking." In contrast, resonant interaction theory (McComas and Bretherton, 1977) suggests that these waves are unstable in some sense even at small amplitude. It would seem unnatural to call the latter process "breaking." A kind of theoretical vacuum presently exists between the small- and large-amplitude cases, which is open to study. Future research will hopefully guide us to an exact concept of dynamical wavebreaking.

Second, the "equi"-partition of kinetic and thermal wave action in the inertia-gravity wave (see Appendix) suggests that radiative damping is relatively small compared to, say, viscous damping as $|\hat{\omega}| \rightarrow |f|$. Since it seems more natural to attribute viscous damping to the breaking of otherwise conservative inertia-gravity waves (as Holton, 1982, did for simple waves) our discussion in this section has neglected turbulent forms of wave dissipation.

5. Interpretation of results

The formation of a caustic in Figs. 3–5 can be attributed to the horizontal shear. At least that is what is taught by the simplest example imaginable: the ray equations for simple stationary gravity waves have analytic solutions when the (unidirectional) mean wind is a *separable* function of latitude and height:

$$\bar{u}(y, z) = UF(y)G(z) \quad (5.1)$$

viz.,

$$\int \frac{dz}{G} = \frac{kU}{N} \int \frac{F^2 dy}{F_0[(F/F_0)^2 - 1]^{1/2}} \quad (5.2)$$

when $l_0 = 0$. The left-hand side of (5.2) is just a transformed z -coordinate. When F is linear, i.e., $UF = \Lambda y$, then

$$\int \frac{dz}{G} = \frac{1}{2} \frac{k\Lambda}{N} y_0^2 \times \left\{ \cosh^{-1} y/y_0 + \frac{y}{y_0} [(y/y_0)^2 - 1]^{1/2} \right\} \quad (5.3)$$

which may be shown to have a caustic when $G = 1$. Analytic solutions can also be found on an f -plane.

When combined with another reflecting surface, such as another caustic, a *waveguide* is formed. In a

waveguide, *normal modes* satisfy some *quantization condition*. However, normal mode theory would not seem relevant for inertia-gravity waves in the present context. Waveguides, if they exist at all, are probably quite “leaky” especially taking into account zonal and temporal variations of the basic state. It will be of interest to see if observations confirm this speculation.

The critical layer behavior found in Figs. 3–5 seems to defy explanation in terms of a conventional wisdom that looks for explicit critical “levels” as loci of singular and/or asymptotic behavior. Even the generalized critical surface of Olbers (1981)

$$\hat{\omega} = \omega_\infty \equiv \pm \left[\frac{N^2 \bar{u}_y^2 + f^2 \bar{u}_z^2}{\bar{u}_y^2 + \bar{u}_z^2} \right]^{1/2} \quad (5.4)$$

does not seem very relevant since it is derived from the asymptotic condition du/dt along a ray, and in any case requires constant shear. The ray behavior in Figs. 3–5 is nowhere asymptotic (at least not those rays that have been shown) since the ray times are finite everywhere within the cone. There is also a dependence on the initial wavevector orientation. Obviously these examples serve to reinforce the practical point that wavebreaking is not necessarily, if ever, limited to the immediate vicinity of a critical surface. The pioneering work of Yamanaka and Tanaka (1984a,b) has also demonstrated this.

Acknowledgment. The author thanks N. Butchart, D. C. Fritts, J. R. Holton, W. L. Jones, M. E. McIntyre, and M. D. Yamanaka for helpful discussions and comments on an earlier version of this manuscript. This research was supported by the National Science Foundation, Division of Atmospheric Sciences, Grant NSF-8217503, and by the Air Force Office of Scientific Research, Contract F49620-83-C-0061.

APPENDIX

Perturbation equations for hydrostatic, Boussinesq inertia-gravity waves on a steady, balanced zonal mean flow are

$$D_t u' - f v' + \phi'_x = X' \quad \left(D_t \equiv \frac{\partial}{\partial t} + \bar{u} \frac{\partial}{\partial x} \right) \quad (A.1a)$$

$$D_t v' + f u' + \phi'_y = Y' \quad (A.1b)$$

$$D_t \phi'_z - f v' \bar{u}_z + w' N^2 = Q' \quad (A.1c)$$

$$u'_x + v'_y + w'_z = 0. \quad (A.1d)$$

Following Andrews and McIntyre (1976) and their notation, linear displacement fields appropriate to this problem are

$$D_t \xi' \equiv u' \equiv u' + \eta' \bar{u}_y + \zeta' \bar{u}_z \quad (A.2a)$$

$$D_t \eta' \equiv v' \quad (A.2b)$$

$$D_t \zeta' \equiv w'. \quad (A.2c)$$

We now present the results of three derivations, leaving intermediate steps for the reader.

1. Virial theorem

Multiplying ξ', η' into (A.1a, b) and assuming the rhs is $O(\mu a^2)$ or less, we obtain

$$\bar{u}'^2 + \bar{v}'^2 = \epsilon \bar{\phi}'^2 + 2 \overline{f \eta' u'} + O(\mu a^2) \quad (A.3)$$

where $\epsilon \equiv m^2/N^2$. The gravity wave equipartition between kinetic and available potential energy does not apply to inertia-gravity waves on account of the second term on the rhs of (A.3). In fact, near the inertial frequency cutoff the first term on the rhs is $O(\epsilon^{-1})$ since ϕ' is $O(\epsilon^{-1})$.

2. Wave action law

Multiplying ξ'_x and η'_x into (A.1a,b) and following McIntyre (1980), we obtain for conservative waves

$$\frac{\partial}{\partial t} \{ \overline{\xi'_x (u' - f \eta')} + \overline{\eta'_x v'} \} + \overline{(\eta'_x \phi')_y} + \overline{(\zeta'_x \phi')_z} = 0 \quad (A.4)$$

at first order. Therefore with the help of (A.2a, b) and (A.3) it follows that

$$\frac{\partial}{\partial t} \left\{ \frac{1}{2} \frac{\overline{u'^2 + v'^2 + \epsilon \phi'^2}}{c - \bar{u}} \right\} + \left(\frac{\overline{v' \phi'}}{c - \bar{u}} \right)_y + \left(\frac{\overline{w' \phi'}}{c - \bar{u}} \right)_z = 0. \quad (A.5)$$

To relate the flux of wave action to its density we may proceed directly from the wave equations after substituting the usual monochromatic linear wave form $\exp i(kx - \omega t)$:

$$M_{ij} U_j = 0, \quad (A.6a)$$

where

$$M_{ij} \equiv \begin{pmatrix} -\hat{\omega} & if & k \\ -if & -\hat{\omega} & l \\ k & l & -\epsilon \hat{\omega} \end{pmatrix}, \quad (A.6b)$$

$$U_j \equiv \begin{pmatrix} u \\ v \\ \phi \end{pmatrix}. \quad (A.6c)$$

Differentiation with respect to l (for the meridional flux component) and with respect to ϵ (for the vertical flux component) and making use of the hermitian properties of M_{ij} yields the standard result

$$\overline{v' \phi'} = v_g E; \quad \overline{w' \phi'} = w_g E \quad (A.7a,b)$$

from which (4.1) is obtained.

3. Saturated wave action density

When the mean flow shear is small, as in the WKB approximation, Kelvin–Helmholtz instability is expected when

$$\text{Ri} \equiv \frac{N^2 + \phi'_{zz}}{|\mathbf{u}'_z|^2} < \frac{1}{4}. \quad (\text{A.8})$$

For zonal waves, $\text{Ri} = 0.25$ at the point of minimum static stability when¹

$$\sigma^2 = \frac{0.25a^2}{1-a} + 1 \quad (\text{A.9})$$

where

$$\hat{\omega} \equiv \sigma f \quad (\text{A.10a})$$

$$u' \equiv \hat{c}a \sin \Phi. \quad (\text{A.10b})$$

Obviously we must be quite close to the inertial frequency cutoff before a becomes significantly less than 1 (= direct convective breaking)—for example, $a = 0.5$ when $\sigma = 1.06$. Letting $a_s(\sigma)$ denote the value of a satisfying (A.9), solving for \hat{A}_s , we obtain

$$k\hat{A}_s = \frac{1}{2} a_s(\sigma)^2 \hat{c} \quad (\text{A.11})$$

which approaches zero at the inertial frequency.

As noted in the text these arguments neglect mean flow shear which would presumably make K–H instability even more relevant for gravity and inertia-gravity wave breakdown. Of course, the entire role of dynamical instability in gravity and inertia-gravity wave saturation must be established theoretically before these saturation arguments can be justifiably used in models of the atmosphere.

¹ For the values of a required for dynamical wavebreaking Ri is in fact minimum at this point, although this is not necessarily the case for smaller wave amplitudes.

REFERENCES

- Acheson, D. J. 1973: Valve effect of inhomogeneities on anisotropic wave propagation. *J. Fluid Mech.*, **58**, 27–37.
- Andrews, D. G., and M. E. McIntyre, 1976: Planetary waves in horizontal and vertical shear; the generalized Eliassen–Palm relation and the mean zonal acceleration. *J. Atmos. Sci.*, **33**, 2031–2048.
- , and —, 1978: On wave action and its relatives. *J. Fluid Mech.*, **89**, 647–664.
- Barat, J., 1983: The fine structure of the stratospheric flow revealed by differential sounding. *J. Geophys. Res.*, **88**, 5219–5228.
- Cadet, D., and H. Teitelbaum, 1979: Observational evidence of internal inertia-gravity waves in the tropical stratosphere. *J. Atmos. Sci.*, **35**, 892–907.
- Dunkerton, T. J., 1982a: Wave transience in a compressible atmosphere, part 3: the saturation of internal gravity waves in the mesosphere. *J. Atmos. Sci.*, **39**, 1042–1051.
- , 1982b: Stochastic parameterization of gravity wave stresses. *J. Atmos. Sci.*, **39**, 1711–1725.
- , and N. Butchart, 1984: Propagation and selective transmission of internal gravity waves in a sudden warming. *J. Atmos. Sci.*, **41**, 1443–1460.
- Fels, S. B., 1982: A parameterization of scale-dependent radiative damping rates in the middle atmosphere. *J. Atmos. Sci.*, **39**, 1141–1152.
- Fritts, D. C., 1984: Gravity wave saturation in the middle atmosphere: A review of theory and observations. *Rev. Geophys. and Space Phys.*
- Grimshaw, R., 1975: Internal gravity waves: critical layer absorption in a rotating fluid. *J. Fluid Mech.*, **70**, 287–304.
- , 1980: A general theory of critical level absorption and valve effects for linear wave propagation. *Geophys. Astrophys. Fluid Dynamics*, **14**, 303–326.
- Holton, J. R., 1982: The role of gravity wave-induced drag and diffusion in the momentum budget of the mesosphere. *J. Atmos. Sci.*, **39**, 791–799.
- Ivanov, Yu. A., and Ye. G. Morozov, 1974: Deformation of internal gravity waves by a stream with horizontal velocity shear. *Okeanologie*, **14**, 457–461.
- Jones, W. L., 1967: Propagation of internal gravity waves in fluids with shear flow and rotation. *J. Fluid Mech.*, **30**, 439–448.
- , 1969: Ray tracing for internal gravity waves. *J. Geophys. Res.*, **74**, 2028–2033.
- Kitchen, E. H., and M. E. McIntyre, 1980: On whether inertia-gravity waves are absorbed or reflected when their intrinsic frequency is doppler-shifted towards f . *J. Meteor. Soc. Japan*, **58**, 118–125.
- Lighthill, M. J., 1978: *Waves in Fluids*, Cambridge University Press.
- Lindzen, R. S., 1981: Turbulence and stress due to gravity wave and tidal breakdown. *J. Geophys. Res.*, **86C**, 9707–9714.
- McComas, C. H., and F. P. Bretherton, 1977: Resonant interaction of oceanic internal waves. *J. Geophys. Res.*, **82**, 1397–1412.
- McIntyre, M. E., 1980: An introduction to the generalized Lagrangian-mean description of wave, mean-flow interaction. *Pure and Appl. Geophys.*, **118**, 152–176.
- , 1981: How well do we understand stratospheric warmings? *J. Meteor. Soc. Japan*, **60**, 37–65.
- , and T. N. Palmer, 1983: Breaking planetary waves in the stratosphere. *Nature*, **305**, 593–600.
- Mooers, C. N. K., 1975a: Several effects of baroclinic currents on the three-dimensional propagation of inertial-internal waves. *Geophys. Fluid Dyn.*, **6**, 277–284.
- , 1975b: Several effects of a baroclinic current on the cross-stream propagation of inertial-internal waves. *Geophys. Fluid Dyn.*, **6**, 245–275.
- Olbens, D., 1981: The propagation of internal waves in a geostrophic current. *J. Phys. Ocean.*, **11**, 1224–1233.
- Sato, T., and R. Woodman, 1982: Fine altitude resolution observations of stratospheric turbulent layers by the Arecibo 430 MHz radar. *J. Atmos. Sci.*, **39**, 2546–2552.
- Sawyer, J. S., 1960: Quasi-periodic wind variations with height in the lower stratosphere. *Quart. J. Roy. Meteor. Soc.*, **87**, 24–33.
- Smith, S. A., and D. C. Fritts, 1983: Estimation of gravity wave motions, momentum fluxes, and induced mean flow accelerations in the winter mesosphere over Poker Flat, Alaska. *Proc. 21st Conf. Radar Meteor.*, Edmonton, Amer. Meteor. Soc. (in press).
- Thompson, R. O. R. Y., 1978: Observation of inertial waves in the stratosphere. *Quart. J. Roy. Meteor. Soc.*, **104**, 691–698.
- Vincent, R. A., and I. M. Reid, 1983: HF Doppler measurements of mesospheric gravity wave momentum fluxes. *J. Atmos. Sci.*, **40**, 1321–1333.
- Yamanaka, M. C., and H. Tanaka, 1984a: Multiple “gust layers” observed in the middle stratosphere. *Dynamics of the Middle Atmosphere*, 117–140.
- , and —, 1984b: Propagation and breakdown of internal inertia-gravity waves near critical levels in the middle atmosphere. *J. Meteor. Soc. Japan*, **62**, 1–16.